THE FORMATION OF GIANT RADIATING DIKE SYSTEMS ON VENUS: INSIGHTS FROM ELASTOPLASTIC FLEXURAL MODELS. Gerald A. Galgana[1], Patrick J. McGovern[1] and Eric B. Grosfils[2]; [1]Lunar and Planetary Institute, USRA, 3600 Bay Area Blvd., Houston, TX 77058; (galgana@lpi.usra.edu; mcgovern@lpi.usra.edu); [2]Geology Department, Pomona College, Claremont, CA 91711(egrosfils@pomona.edu).

Introduction. Giant radiating dike systems are enigmatic volcano-tectonic features broadly distributed across the surface of Venus. These prominent structures are identified through a centrally located topographic feature, from which fractures fan outward to an average of 325 km radius, but some extend to 2,000 km [1]. These systems are theorized to originate from extensional stresses in the upper lithosphere caused by mantle upwelling, or through stresses due to lateral emplacement of dikes from shallow central magma reservoirs within the lithosphere [1-7]. Testing these ideas we showed previously how reservoir inflation and lithospheric flexure can combine to drive wall fracture and the intrusion behavior needed to explain how such systems might form [8-11]; our mechanical models use internally pressurized magma chambers embedded in a gravitationally loaded Venusian lithosphere that responds flexurally to upward-directed stresses from a rising mantle diapir; the nature and orientation of principal stresses in the lithosphere and along the magma chamber walls dictate the rock failure patterns, and hence influence the intrusion of magmatic material. Here, using finite element (FE) models, we examine variations introduced when more realistic material behavior (i.e., elastoplasticity) is used to define the lithosphere and associated reservoir wall failure modes. We then analyze the implications for dike formation, magma ascent and lateral propagation.

Method. We develop gravitationally loaded, axisymmetric FE models (with lithostatic prestress) of the Venusian lithosphere (T_e = 20 km; lithosphere radius L_r = 900 km). Horizontal movement is constrained at the distal part of the model, while Winkler restoring forces are imposed at the bottom of the lithosphere to simulate the effects of buoyant support from the mantle asthenosphere. Uplift is represented by a 3 km thick by 200 km radius conical load (representing, for example, the initial stages of plume contact) applied at the symmetry axis. Using this setup, we model brittle failure of the lithosphere via plastic yielding using the Drucker-Prager criterion [12], a numerically tractable approximation to the Mohr-Coulomb criterion, and calculate stresses in the modeled lithosphere. To further observe stress interactions in the upper lithosphere, spherical magma chambers (r = 1 km, modeled as magma-filled cavities) are embedded in separate models at two different depths: upper (D_{tC} = 4 km) and near mid-lithosphere (D_{tC} = 7 km). These reservoirs are then incrementally pressurized to the point of failure, i.e. failure occurs when the actual material strength (elastic) limit is reached. From the loading conditions, we predict failure locations from reservoir wall stresses and plots showing regions of plastic yielding; we also determine the modes of magma intrusions based on predicted fracture orientations. We interpret the likelihood of magma ascent within the lithosphere based on the spatial distribution of failed regions caused by excessive stresses as well as the orientation of principal stress axes within the lithosphere.

Results. In our previous elastic models [10], coupled chamber pressurization and lithospheric flexure induced failure at the crest of upper lithosphere reservoirs, while reservoirs situated within the lower lithosphere tended to fail at their midsections. However, introduction of plastic yielding creates distinctive changes in lithospheric and chamber margin stress states. Specifically, the typical flexural profile of "differential tectonic" stress (radial component $\sigma_{DTr} = \sigma_r - \sigma_z$), a linear increase becoming more extensional with increasing height, is altered by plastic strain such that σ_{DTr} decreases to near zero at the top of the lithosphere (red line in Fig. 1). Chamber-margin stresses are also affected: the formerly concave or "banana-shaped" profiles (Fig. 2, red and blue lines) are blunted near the crest (indicating stress relief due to plastic yielding), with the failed region progressively moving downward along the margin with increasing reservoir overpressures (P_{over}). Further, the most extensional stress (σ_E) component is still increasing (moving toward positive stress). As P_{over} is elevated further, the entire chamber margin fails, at which point the "banana" shape of the stress curves has completely changed to a prolate (or "American football") shape (Fig. 2, green and pink lines). Further increases in P_{over} actually decrease σ_E, moving the stress state away from the tensile region (i.e., the zero stress line).

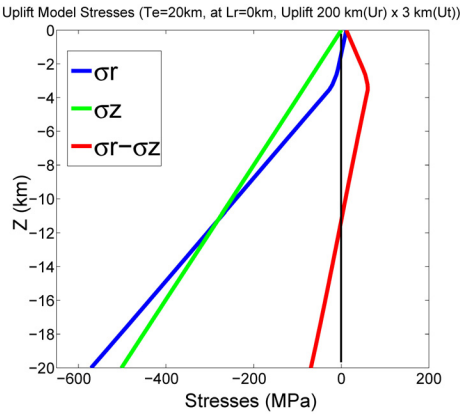

Figure 1. Radial (σ_r, blue), vertical (σ_z , green) and differential tectonic (σ_{DTr}, red) stresses vs. depth z at r = 0. Note relief of stress via plastic strain at top of the 20 km thick lithosphere.

Discussion. Overall, when compared to elastic end-member results, elastoplastic models show considerable differences in stress concentration/strain localization, producing a different evolutionary pattern of lithosphere and reservoir failure. Upon uplift, the upper region of the lithosphere immediately reaches material failure; the resulting change of sign in the differential tectonic stress vertical gradient (Fig. 1) inhibits magma ascent [13], perhaps contributing to the trapping of radial dikes in the upper lithosphere and encouraging their outward propagation [cf. 10]. Upper lithosphere yielding also affects chamber boundary stresses, creating the "stem" of the banana-shaped stress profile in Figure 2 that moves reservoir failure away from the top of the chamber. The specifics of the chosen failure envelope exert a significant effect. A "Byerlee-type" [14] envelope, with low values of cohesion and friction angle, represents frictional sliding of a large rock mass along abundant fractures with a wide variety of orientations to serve as potential fault planes. For such an envelope, it is difficult to reach the tensile regime at the chamber boundary (Fig. 3, upper). On the other hand, criteria for Coulomb fracture of more-or-less intact rock (derived from laboratory experiments) have higher cohesion and friction angle values, making it possible to achieve tensile chamber-boundary stresses (Fig. 3, lower). To be strictly consistent tensile failure criterion, the σ_E end of the Mohr circle should be in contact with the tensile strength of the material, i.e., the apex of the failure envelope at shear stress $\tau = 0$. This situation is not strictly possible for simple linear criteria (an infinitesimally small Mohr circle would be required), but curved criteria such as those derived from Griffith fracture theory (e.g., [15] or Hoek-Brown rock-mass strength ratings [16]) would allow finite circles to intersect at or near the tensile strength.

The interaction of the yield criteria with chamber depth also matters. For a shallow chamber (D_{tC} = 4 km), the initial chamber stress state is relatively close to the tensile regime, and modest P_{over} can push it near or into tensile stress (Fig. 2). For a deeper chamber (i.e., D_{tC} = 7 km), the stresses lie far from the tensile regime (particularly for σ_z) initially, and as increases in P_{over} push σ_E toward extension the Mohr circle intersects the failure envelope well short of tensile σ_E. After the entire chamber margin is in failure, further increases in P_{over} simply move σ_C and σ_E toward greater compression. Thus, deep chambers may never strictly satisfy a tensile failure criterion, and therefore are less likely to issue organized intrusive systems like dike swarms from their margins. Instead, shear failure of the chamber margin may allow magma to infiltrate the country rock, either by intruding fault planes [e.g., 17] or by stoping fractured rock into the chamber. The latter may be a means of effective chamber expansion: chambers predicted to fail at their crests would become more prolate (taller), and chambers that fail in their middles would become more oblate (wider). The resulting geometric alterations favor stress concentrations that will further influence the progress of magmatic intrusion. Additional factors not yet introduced within our models, such as vertical or lateral heterogeneity within the lithosphere may also influence radial dike formation and volcanic center evolution.

References. [1] Grosfils, E. and J. Head (1994) *GRL,* 21(8): 701-704. [2] Stofan, E. et al. (1992) *JGR*, 97:13,347-13,378. [3] Koch D. and M. Manga (1996) *GRL*, 99:225-228.[4] Krassilnikov, A. and J. Head (2003) *JGR,* 108(E9), 5108. [5] Janes, D. and S. Squyres (1993) *GRL* 20(24):2,961-2,964. [6] Cyr, K. and H. Melosh (1993) *Icarus*, 102:175-184. [7] Parfitt, E. et al. (1993) *JVGR*, 55(1-2). [8] Grosfils, E. (2007) *JVGR*, 166: 47-75. [9] Hurwitz, D., et al. (2009) *JVGR*, 188:379-394. [10] Galgana, G. et al. (2010) *LPSC XLI*, 1777. [11] Galgana, G. et al. (2011) *JGR*, doi:10.1029/2010JE 003654. [12] Drucker, D. and W. Prager (1952) *Q. Appl. Math* 10(2):157-169. [13] Rubin A. (1995) *Annu. Rev. Earth Planet. Sci.*, 23:287-336. [14] Byerlee, J. (1978) *Pure Appl. Geophys.,* 116(405):615-626. [15] Suppe, J. (1985) *Structural Geology*, Prentice Hall, NJ, 537p. [16] Hoek, E., and E Brown (1980) *J. Geotech. Eng. Div. Am. Soc. Civ. Eng., 106*:1013-1035. [17] Galland, O. et al. (2007) *J. Geophys. Res., 112*, doi:10.1029/ 2006JB004604.

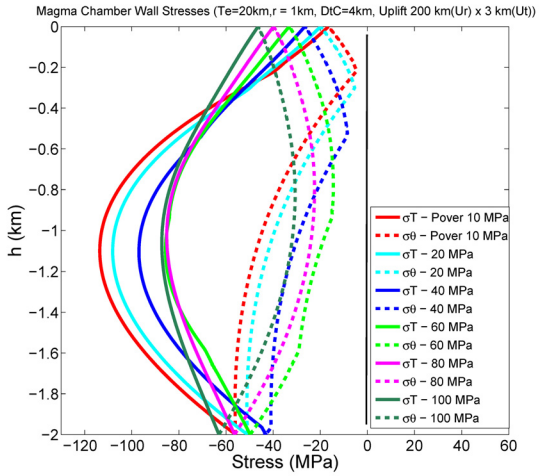

Figure 2. Tangential (σT, solid lines) and out-of-plane ($\sigma\theta$, dashed lines) normal stresses along the magma chamber wall (distances expressed as depth h beneath the crest of magma chamber), for an upper lithosphere chamber (depth (D_{tC}) = 4 km) with increasing pressurization (legend).

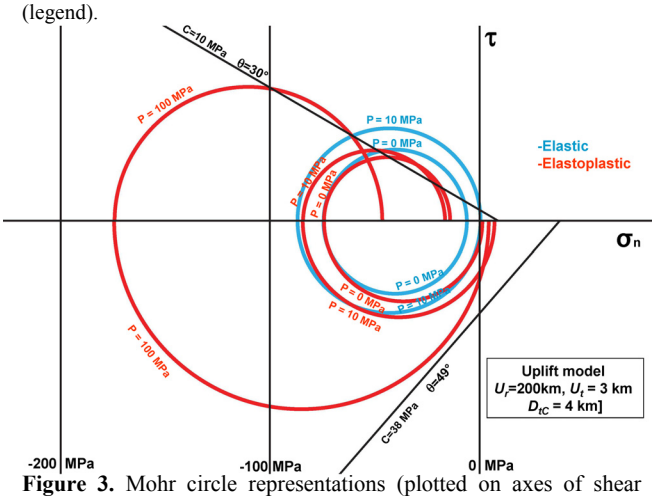

Figure 3. Mohr circle representations (plotted on axes of shear stress τ vs. normal stress σn) of stress states at the apex of a 1-km-radius magma chamber from elastic (blue) and elastoplastic (red) models of coupled chamber inflation and lithospheric flexure (D_{tC} = 4 km). Chamber overpressure values P indicated for each circle. Largest P value for elastic models corresponds to boundary of tensile region (σn = 0). Upper half: elastoplastic model stress state for a "Byerlee-type" failure envelope (black line) with low values of friction angle (30°) and cohesion (10 MPa); Lower half: "intact rock-type" failure envelope for high values of friction angle (49°) and cohesion (38 MPa).